Spin spiral order induced ferroelectricity in $MnRe_2O_8$ monolayer

Shiqiang Yu, Yushuo Xu, Ying Dai,* Dongyue Sun, Baibiao Huang, and Wei Wei†
School of Physics, State Key Laboratory of Crystal Materials, Shandong University, Jinan 250100, China

(Received 25 July 2023; accepted 7 November 2023; published 17 November 2023)

In this work, on the basis of first-principles calculations we demonstrate that magnetic exchange frustration caused spin spiral can generate an electric polarization ($31.46\,\mu C/m^2$) in two-dimensional (2D) $MnRe_2O_8$, which, therefore, can be identified as a very rare type-II multiferroic material with robust magnetoelectric coupling. It is of high interest that the ferroelectricity is out of plane, explained by the mechanism of $\boldsymbol{P} \propto \boldsymbol{S}_a \times \boldsymbol{S}_b$ in the generalized spin-current model. We propose that compressive strain can improve the Néel temperature (from 31 to 63 K) as well as the electric polarization in terms of enhancing the supersuperexchange interaction for this in-plane noncollinear 120°-ordered antiferromagnetic order. The spin spiral chirality can be flexibly switched by a vertical electric field, that is, the polarization-chirality locking effect. It can be confirmed conclusively that our findings deepen the understanding on the magnetoelectric physics, and open a different avenue for magnetoelectric and magneto-optical applications based on 2D type-II multiferroic materials.

DOI: 10.1103/PhysRevB.108.174429

I. INTRODUCTION

In recent years, we have witnessed the rapid development of two-dimensional (2D) materials; the fundamental physics in conventional materials have found their analogies in two dimensions [1–4]. In particular, ferroicity with switchable magnetic, polar, or elastic orders has also been validated in materials in 2D form [5–8]. It is of high interest and great importance that in multiferroic materials the coupled magnetism and polarization could be manipulated by external field: magnetic field governs the electric polarization and electric field regulates magnetic phase transition. It therefore refers to the fundamental magnetoelectric physics in 2D systems and high-performance magnetoelectric and magneto-optical applications [9–11]. It has to be noted that, however, 2D multiferroic materials with robust magnetoelectric coupling are extremely rare; this is due to the inherent repulsion between magnetism and polarization in the occupation of metal *d* orbitals. In previous studies, some 2D multiferroics with magnetoelectric coupling such as VOI_2, Tl_2NO_2, and $FeHfSe_3$ were theoretically predicted [12–15], and extremely rare examples have been experimentally verified. It has been demonstrated experimentally that, for instance, $CuCrP_2S_6$ nanosheet exhibits electric polarization and magnetic hysteresis loops [16]. In addition, the coexistence of ferrimagnetism and ferroelectricity in Fe-doped α-In_2Se_3 and *p*-type SnSe verifies their multiferroic feature [17,18]. In addition to monolayer (ML) cases, constructing ferroelectric/ferromagnetic heterostructures is another way to obtain magnetoelectric coupling properties. In 2023, a pioneering multiferroic heterostructure composed of 2D ferromagnetic $Cr_2Ge_2Te_6$ and thin ferroelectric polymer was reported. In light of the interfacial multiferroic effect, the hysteresis loop of $Cr_2Ge_2Te_6$ bilayer (BL) can be modulated by applying electric field [19]. It should be pointed that experimentally reported 2D multiferroics are just limited to the above-mentioned materials. In these candidates, the magnetism and electric polarization derive from different sources (i.e., type-I multiferroics), giving rise to rather weak magnetoelectric coupling and thus severally limiting the practical applications.

In an alternative way, noncollinear magnetic structure can also provide a promising possibility to achieve robust magnetoelectric coupling [20–23]. In general, the noncollinear spin configurations arise from the magnetic exchange frustration in triangular lattices, leading to distinct spin orders in consideration of spin-orbit coupling (SOC); for instance, proper-screw, cycloidal, and 120° (or Y-type) noncollinear antiferromagnetic (AFM) orders [24–29]. The noncollinear magnetic structure spontaneously breaks the spatial inversion symmetry and time-reversal symmetry, and, therefore, instigates nondisplacive electric polarization and a nonlinear interaction between magnetism and polarization. In addition, helical spin structure endows the material a new quantum state, namely, the spin spiral chirality, which is the root for the Hall effect sign change and can be switched [30–32]. The inherently coupled magnetism and ferroelectricity (type-II multiferroicity) signifies large magnetoelectric effects.

Although type-II multiferroicity can exist in bulk materials with noncollinear AFM state, it is extremely rare in 2D cases. This is because these bulk structures cannot be thinned to the 2D forms, and, additionally, reducing the thickness to nanoscale will also alter the magnetic properties. In previous investigations, very few examples of noncollinear spin order induced ferroelectricity in 2D materials have been verified for $Hf_2VC_2F_2$ and NiI_2 [33,34]. In these type-II multiferroic candidates, the induced electric polarization is however in-plane, losing the opportunity to be electrically controllable. They also suffer from either small polarization or low

*Corresponding author: daiy60@sdu.edu.cn
†Corresponding author: weiw@sdu.edu.cn

critical temperature. In this view, therefore, it is fundamental in physics and interesting for applications to find new 2D type-II multiferroic materials with strong magnetoelectric coupling, which is currently still a huge challenge.

In the present work, based on first-principles calculations, we reveal that an out-of-plane ferroelectricity can be induced by an in-plane noncollinear 120°-ordered AFM spin spiral in $MnRe_2O_8$ ML, conforming its promising type-II multiferroicity and robust intrinsic magnetoelectric coupling. In particular, the switchable polarization can be stabilized by the presence of a band gap. In accordance to the geometry feature of $MnRe_2O_8$ ML, we propose that compressive strain can enhance the Néel temperature as well as the electric polarization in terms of enhancing the supersuperexchange interaction. Because of the out-of-plane polarization, a vertical electric field enables the switching of the spin spiral chirality, giving rise to a polarization-chirality locking effect and realizing electrically controllable magnetism. In addition, the pivotal role of SOC is discussed. It thus can be confirmed conclusively that $MnRe_2O_8$ ML provides a promising platform for studying the magnetoelectric physics in two dimensions, and offers unprecedented opportunities for exploring the cutting-edge devices in nanoscale.

II. COMPUTATIONAL METHODS

First-principles calculations were performed based on the density functional theory (DFT) using the projector augmented wave (PAW) method, as implemented in the Vienna *Ab Initio* Simulation Package (VASP) [35,36]. For the exchange-correlation functional, the generalized gradient approximation (GGA) in the form of Perdew-Burke-Ernzerhof (PBE) was employed [37]. An effective Hubbard $U = 4$ eV was added for Mn-3*d* orbitals, which were frequently used in previous works [38,39]. The Monkhorst-Pack *k*-point meshes of $11 \times 11 \times 1$ and $7 \times 7 \times 1$ were employed to sample the two-dimensional (2D) Brillouin zone for the unit cell and $\sqrt{3} \times \sqrt{3} \times 1$ supercell, respectively [40]. The energy cutoff for the plane wave basis was set to 520 eV. A vacuum space of larger than 15 Å was adopted to eliminate the adjacent interactions. The lattice constant and the atomic positions were fully optimized until the force on each atom was less than -0.01 eV/Å and energy tolerance was smaller than 10^{-5} eV. In addition, SOC was considered. In addition, the phonon dispersion spectra of $MnRe_2O_8$ MLs with different magnetic structures were calculated by the PHONOPY code based on density functional perturbation theory to confirm the dynamical stability [41], and the thermal stability was evaluated at 300 K by the *ab initio* molecular dynamics (AIMD) calculations. In the light of the Heisenberg spin Hamiltonian model, Monte Carlo (MC) simulations with the Metropolis algorithm were performed on a $24 \times 24 \times 1$ supercell for each temperature to estimate the thermal dynamics of the magnetism in the equilibrium state. In addition, specific heat capacity can be calculated according to the dissipation-fluctuation theorem, defined as $C_v = (\langle E^2 \rangle - \langle E \rangle^2)/k_B T^2$, with its peak point corresponding to the transition temperature [42]. In respect to the MC simulations, the MCSOLVER package was used, and the magnetic moment and specific heat were measured after the system reaches the equilibrium state with at least 10^6 simulation steps [43–45].

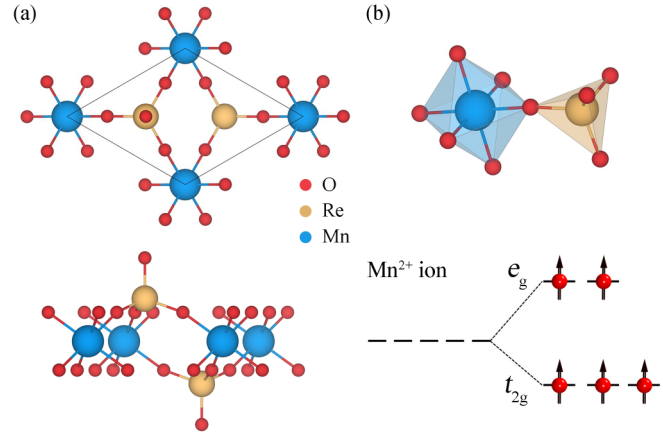

FIG. 1. (a) Top and side views of the crystal structure of $MnRe_2O_8$ ML. (b) ReO_4 tetrahedra and MnO_6 octahedra, and the corresponding energy level diagram of Mn-3*d* orbitals under an octahedral crystal field.

III. RESULTS AND DISCUSSION

In the 1990s, the anhydrous perrhenate $MnRe_2O_8$ of layered crystal structure was successfully synthesized [46,47]. In bulk phase, $MnRe_2O_8$ single layers are combined by weak van der Waals (vdW) interactions with a comparable cleavage energy to graphite, suggesting that the layered structure can be easily thinned to the 2D form with great possibility [38]. In Fig. 1(a), $MnRe_2O_8$ ML structure is presented. It can be found that $MnRe_2O_8$ ML is composed of seven atomic layers arranged vertically as O-Re-O-Mn-O-Re-O with the space group of *P*3_M1. The 2D framework is connected by corner-sharing ReO_4 tetrahedra and MnO_6 octahedra, as shown in Fig. 1(b). In the middle atomic plane, Mn atoms form a triangular lattice with the nearest-neighbor (NN) Mn-Mn distance being 5.89 Å, consistent with experimental results [47]. It is already widely known that the octahedral crystal field categorizes Mn-3*d* orbitals into two groups: triply degenerate t_{2g} states (d_{xy}, d_{xz}, and d_{yz}) and doubly degenerate e_g states ($d_{x^2-y^2}$ and d_{z^2}), Fig. 1(b). In this view, the 3*d* orbitals of Mn^{2+} ion will be featured as a half occupation, which consequently gives rise to a magnetic moment of 5 μ_B (high spin state) and a total spin quantum number of 5/2. Furthermore, the thermal stability of $MnRe_2O_8$ ML is confirmed through the AIMD results; see Fig. S1 of the Supplemental Material [48].

In order to address the magnetic ground state for $MnRe_2O_8$ ML, spin configurations of collinear ferromagnetic (FM), antiferromagnetic (AFM), down-up-up type FM (DUU FM), and noncollinear 120°-rotated AFM (*Y*-AFM) are taken into account [31]; see Figs. 2(a)–2(d). In Table S1 of the Supplemental Material [48], energy comparison between different out-of-plane and in-plane magnetic structures indicates that the magnetic ground state of $MnRe_2O_8$ ML turns out to be in-plane *Y*-AFM order, as in its bulk phase [38]. In Fig. S2 [48], the phonon band structures of $MnRe_2O_8$ ML with considered

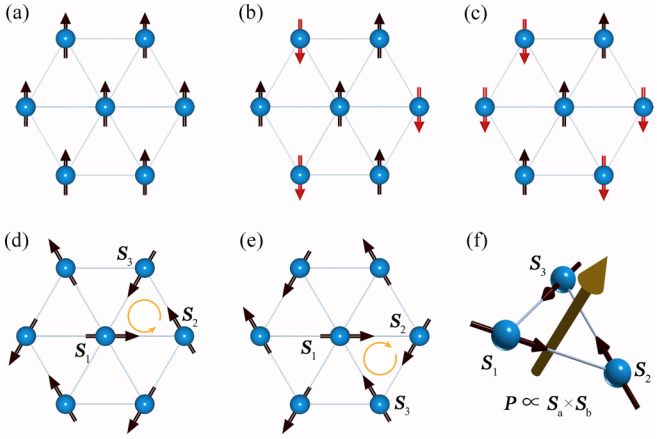

FIG. 2. (a) Out-of-plane collinear ferromagnetic (FM), (b) down-up-up type FM (DUU FM), (c) antiferromagnetic (AFM), and in-plane noncollinear 120°-rotated AFM (*Y*-AFM) order of $MnRe_2O_8$ ML with (d) outward and (e) inward spin spiral chirality. Two noncollinear magnetic states are energetically degenerate. In FM, DUU FM, and AFM configurations, spin directions are out of plane. (f) Schematic of spin spiral induced electric polarization.

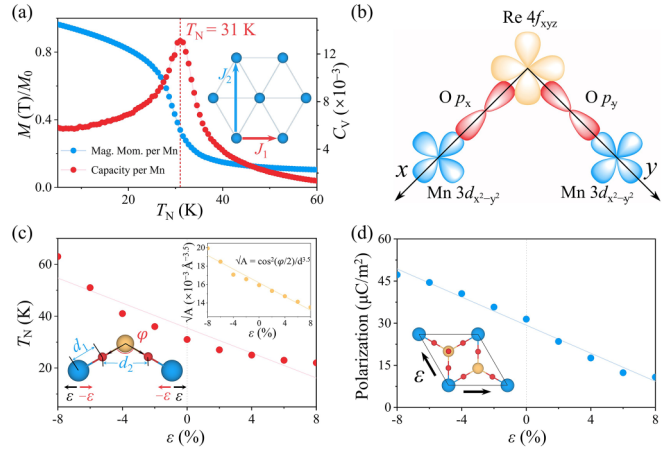

FIG. 3. (a) Normalized magnetization and specific heat as a function of temperature from Monte Carlo simulations. (b) Orbital configurations related to supersuperexchange interactions. (c) Néel temperature as a function of strain. Insets represent the dependence of factor $\sqrt{A}$ on strain, and the definition of relevant geometry parameters. (d) Electric polarization variation with respect to strain. Inset indicates how the biaxial strain is applied on $MnRe_2O_8$ ML.

magnetic configurations confirm their dynamical stability. It is of interest that the noncollinear *Y*-AFM order indicates two energetically degenerate ground states with opposite spin spiral chirality; see Fig. 2(e). In the light of identical magnetic space group and crystal symmetry, two ground orders exhibit the same electronic properties. In Fig. 2(f), the spin spiral induced electric polarization is schematically shown.

As illustrated in Fig. S3 [48], the band structure of noncollinear *Y*-AFM $MnRe_2O_8$ ML implies an indirect band gap of 3.02 eV, thus avoiding the screening of the static internal field generated by the long-range dipolar order of conductive electrons and ensuring the polarization. The hybridization between Re-5*d* and Mn-3*d* orbitals effectively enhance the SOC, thereby stabilizing the noncollinear *Y*-AFM order, though Re-5*d* electrons do not contribute to the magnetism. For noncollinear *Y*-AFM $MnRe_2O_8$ ML, a spin spiral plane forms and the chirality depends on the easy-magnetization plane.

It is of interest to note that for $MnRe_2O_8$ ML the energy difference between magnetic states of consideration is larger than that in the bulk case [38], indicating an elevated Néel temperature. To unravel the temperature-dependent magnetism of $MnRe_2O_8$ ML, Monte Carlo simulations are performed, and the Heisenberg spin Hamiltonian model is

$$H = -\sum_{\langle ij \rangle} J_1 \boldsymbol{S}_i \boldsymbol{S}_j - \sum_{\langle mn \rangle} J_2 \boldsymbol{S}_m \boldsymbol{S}_n - A \sum_i \left(S_i^{ab}\right)^2,$$

where J_1 is the NN exchange interaction, J_2 is the next-nearest-neighbor (NNN) exchange interaction; $\langle ij \rangle$ and $\langle mn \rangle$ correspond to the NN and NNN Mn atoms, respectively; S stands for the normalized spin operator; A is the magnetocrystalline anisotropy coefficient, and S_i^{ab} is the spin momentum in the *ab* plane. By comparing the energies of different magnetic coupling states, J_1, J_2, and A are calculated to be −2.33, 0.47, and 0.32 meV, respectively. It can be seen that J_1 dominates the noncollinear *Y*-AFM order. Accordingly, the Néel temperature of $MnRe_2O_8$ ML is estimated to be approximately 31 K, as depicted in Fig. 3(a). It is higher than those of bulk multiferroic materials with noncollinear *Y*-AFM and comparable to that of synthesized VI_2 ML [34,49–51].

In principle, the exchange interactions between magnetic cations at the octahedral center can be qualitatively described by the orbital configurations of magnetic cations and nonmagnetic bridging anions [52]. In Fig. 3(b), orbital configuration for the local geometry of $MnRe_2O_8$ ML is shown. In particular, MnO_6 octahedra and ReO_4 tetrahedra are corner-oxygen atom sharing, therefore, two pathways for the supersuperexchange are available: (1) Mn^{2+}-O^{2-}-O^{2-}-Mn^{2+}, and (2) Mn^{2+}-O^{2-}-Re^{7+}-O^{2-}-Mn^{2+}. In the case of path 1, AFM exchange interaction is preferential. In path 2, due to the splitting of Re-4*f* orbitals under the tetrahedral crystal field, the highest-energy f_{xyz} orbital hybridizes with the 2*p* orbitals of O^{2-} ions as bridges, which also leads to the AFM order. In comparison to path 1, path 2 contributes to a weaker AFM exchange interaction due to the extra Re^{7+} ion [53–55]. In Fig. S4 [48], charge density distribution clearly illustrates that path 1 is dominating, that is, the supersuperexchange AFM interaction is achieved through the Mn^{2+}-O^{2-}-O^{2-}-Mn^{2+} path. In addition, the strong hybridization between Mn-$d_{x^2-y^2}$ and O-*p* orbitals shown in the projected density of states (PDOS) also confirms the exchange interaction mechanism. On the other hand, the O^{2-}-O^{2-} distance (2.9 Å) is larger than a typical vdW distance (i.e., 2.8 Å), and the ∠Mn^{2+}-O^{2-}-O^{2-} (135°) is smaller than 160°. In this situation, the supersuperexchange interaction following path 1 is however not strong, which is responsible for the low transition temperature [56].

In order to increase the Néel temperature, we therefore propose an effective strategy for enhancing the AFM interaction through the Mn^{2+}-O^{2-}-O^{2-}-Mn^{2+} path. In a sense, the supersuperexchange interaction strength is governed by the exchange integral J, which is determined by $4t^2/U$, with U and t being the on-site Coulomb repulsion and orbital overlap integral, respectively [55–57]. In particular, t relies

on the bond length between NN atoms. In this view, thus the strength of AFM interaction could be quantitated by both the bond angles and bond lengths. In accordance to Harrison's formula and its extension for the supersuperexchange [55,58], one can find that t is proportional to the factor $\sqrt{A}$. In particular, $\sqrt{A} = \cos^2(\varphi/2)/d^{3.5}$, where d denotes the average bond length of $(2d_1 + d_2)$ and φ refers to the angle of ∠O-Re-O. In Fig. 3(c), the inset clearly shows the relationship between $\sqrt{A}$ and d and φ, and its effectiveness was extensively confirmed in previous works [59–62]. In other words, the magnitude of the orbital overlap integral t hinges upon the values of d and θ. It is therefore conceivable that biaxial compressive strain along the a and b axis can reduce d and θ, then enhance t and strengthen the supersuperexchange interaction, and eventually elevate the Néel temperature. In Fig. 3(c), the Néel temperature of $MnRe_2O_8$ ML in Y-AFM state as a function of strain ε (from -8% to 8%) is shown. In particular, the strain is defined as $\varepsilon = (\frac{l-l_0}{l_0}) \times 100\%$, with l and l_0 being the lattice constants for strained and strain-free structures, respectively. It can be observed that the Néel temperature reaches 63 K under a compressive strain of -8%, twice the value of the strain-free case. It is of also interest that the polarization increases to $47.24\,\mu C/m^2$ under a strain of -8%, as shown in Fig. 3(d). It therefore can be concluded that compressive strain can effectively enhance the Néel temperature as well as the polarization simultaneously for the type-II multiferroic $MnRe_2O_8$ ML.

In accordance to the results from the Berry phase method, Y-AFM $MnRe_2O_8$ ML gives rise to an electric polarization of 0.03 pC/m. It corresponds to a value of $31.46\,\mu C/m^2$ in bulk phase when considering its thickness of 6.74 Å, which is one order of magnitude larger than other noncollinear magnetic materials such as $Ba_3MnNb_2O_9$ ($3.45\,\mu C/m^2$) [23]. It must be pointed out that although the electric polarization of $MnRe_2O_8$ ML is smaller than those of other 2D ferroelectrics such as predicted honeycomb binary buckled compounds ($0.88 - 11.45$ pC/m) [63], Co_2CF_2 (11.70 pC/m) [64], and synthesized $1T'$-ReS_2 (0.07 pC/m) [65], its origin is conceptually different from these ferroelectrics. In general, the electric polarization of type-II multiferroics is indeed weaker than that of ordinary ferroelectrics [33,66]; however, the nontrivial origin of ferroelectricity ensures an intrinsically strong magnetoelectric coupling, a trait seldom found in other multiferroics. In particular, the polarization is entirely derived from the bias of electronic cloud because of the spatial inversion symmetry, signifying the inherent coupling between magnetism and electric polarization in $MnRe_2O_8$ ML. The energy of Y-AFM $MnRe_2O_8$ ML with ab-plane spin spiral is 0.32 meV/unit cell lower than that with ac/bc-plane spin spiral. In this case, it implies that the spin spiral chirality is perpendicular to the material basal plane. It should be highlighted that the electric polarization is parallel to the spin spiral chirality, which, therefore, provides the possibility to switch the spin spiral chirality through an electric field. That is, the magnetism can be electrically controlled.

In general, the electric polarization derived from paired spins can be expressed as a bilinear function of the spin component

$$P^{\alpha}_{1,2} = \sum_{ij} \lambda^{\alpha}_{i,j} S^i_1 S^j_2,$$

where α $(= x, y, z)$ represents the polarization component and i, j represents the spin components; $\lambda^{\alpha}_{i,j}$ denotes the magnetoelectric coupling coefficient determined by the local symmetry of the bonds connecting spin pairs. In consideration of spatial inversion symmetry and time-reversal symmetry, we have $\lambda^{\alpha}_{i,j} = -\lambda^{\alpha}_{j,i}$ and $\lambda^{\alpha}_{i,i} = 0$. As a result, the local electric polarization is

$$\begin{aligned} P^{\alpha}_{1,2} &= \sum_{ij} \lambda^{\alpha}_{i,j} \left(S^i_1 S^j_2 - S^j_1 S^i_2\right) \\ &= \lambda^{\alpha}_{x,y} (\boldsymbol{S}_a \times \boldsymbol{S}_b)_z + \lambda^{\alpha}_{z,x} (\boldsymbol{S}_a \times \boldsymbol{S}_b)_y + \lambda^{\alpha}_{y,z} (\boldsymbol{S}_a \times \boldsymbol{S}_b)_x, \end{aligned}$$

where $(\boldsymbol{S}_a \times \boldsymbol{S}_b)_{\alpha}$ represents the α $(= x, y, z)$ component of the vector $(\boldsymbol{S}_a \times \boldsymbol{S}_b)$. In cases $M_{\alpha x} = \lambda^{\alpha}_{y,z}$, $M_{\alpha y} = \lambda^{\alpha}_{z,x}$, and $M_{\alpha z} = \lambda^{\alpha}_{x,y}$,

$$P^{\alpha}_{1,2} = \sum_{\beta} M_{\alpha\beta} (\boldsymbol{S}_a \times \boldsymbol{S}_b)_{\beta}$$

can be rewritten as matrix product

$$\boldsymbol{P}_{1,2} = \mathbf{M} (\boldsymbol{S}_a \times \boldsymbol{S}_b),$$

where $M_{\alpha\beta}$ is the matrix element of $\mathbf{M}$, and the 3×3 coefficient matrix $\mathbf{M}$ reads

$$\begin{pmatrix} M_{xx} & 0 & 0 \\ 0 & M_{yy} & M_{yz} \\ 0 & M_{zy} & M_{zz} \end{pmatrix}.$$

In the case for $MnRe_2O_8$ ML, we address $\mathbf{M}$ via the first-principles calculations as

$$\mathbf{M} = -\begin{pmatrix} 5.64 & 0 & 0 \\ 0 & 5.64 & 0 \\ 0 & 0 & 6.82 \end{pmatrix} \times 10^{-4}\, e\text{Å}.$$

It can be clearly seen that the magnetoelectric coupling follows the antisymmetric mechanism $\boldsymbol{P} \propto \boldsymbol{S}_{\mathrm{a}} \times \boldsymbol{S}_{\mathrm{b}}$ proposed by Xiang *et al.* [67,68].

In Fig. 4(a), magnetic anisotropy energy (MAE) is shown with the energy of the xy-plane (ab-plane) Y-AFM state set to zero. It is obvious that MAE presents a dependence on the rotation angle, and, therefore, the polarization exhibits a robust coupling with the rotation angle. The MAE reaches maximum 0.32 meV/unit cell when the spin spiral plane is perpendicular to the xy plane (that is, the xz or yz plane). As shown in Fig. 4(b), x- and z-direction polarization displays sine and cosine modulation as a function of the rotation angle, respectively. The x-direction polarization reaches the largest $26.06\,\mu C/m^2$ at 90°, and reverses at 270°. For the z-direction polarization, it maximizes at 0° with a value of $31.46\,\mu C/m^2$, and the polarization as well as the spin spiral chirality reverse at 180°. In this view, the dependence of electric polarization on rotation angle also elucidates that the magnetoelectric coupling in $MnRe_2O_8$ ML follows the antisymmetric mechanism $\boldsymbol{P} \propto \boldsymbol{S}_{\mathrm{a}} \times \boldsymbol{S}_{\mathrm{b}}$ in the generalized spin-current model.

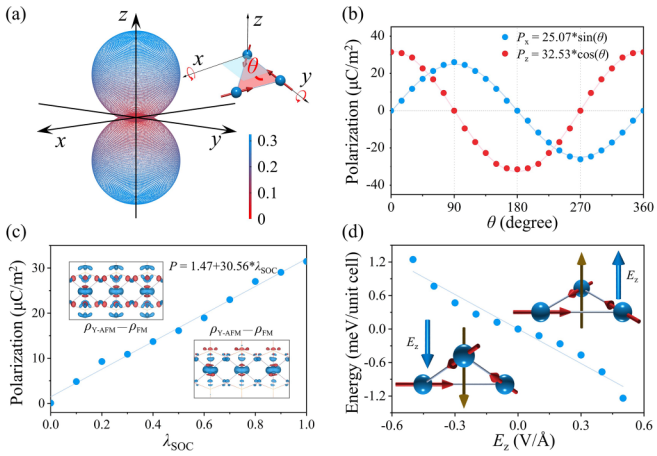

FIG. 4. (a) MAE for $MnRe_2O_8$ ML, the energy of the *ab*-plane *Y*-AFM state is set to zero. Inset defines the rotation angle (θ). (b) Polarization in x and z direction as a function of θ. (c) Polarization as a function of the strength of SOC (λ_{SOC}). Insets represent the charge density differences between *Y*-AFM and FM states with λ_{SOC} being 0 and 1. Red and blue regions indicate charge accumulation and depletion, respectively. The isosurface is set as $5.0 \times 10^{-5}\, e/\text{Å}^3$. (d) Energy difference between two degenerate *Y*-AFM states with opposite spin spiral chirality under external electric field. Insets represent the resultant spin spiral chirality and polarization under external electric field.

In order to verify the crucial role of SOC in magnetoelectric coupling, the relationship between electric polarization and the strength of SOC (λ_{SOC}) is examined and the result is shown in Fig. 4(c). It can be seen that the electric polarization decreases monotonously as λ_{SOC} decreases, and the noncollinear *Y*-AFM state fails to induce polarization when $\lambda_{SOC} = 0$. It reveals a perfect linear relationship between electric polarization and λ_{SOC}, with the coefficient of determination being 0.99. In the case $\lambda_{SOC} = 0$, as shown in the insets to Fig. 4(c), the charge density difference between the *Y*-AFM and FM states is symmetric. As $\lambda_{SOC} = 1$, the charge redistribution turns out to be asymmetric, generating the nondisplacive out-of-plane electric polarization.

It can be found from Fig. 4(d) that the degenerate *Y*-AFM states with opposite spin spiral chirality can be lifted under an external electric field. In the case where the external electric field strength is 0.5 V/Å, the energy difference can reach up to 1.24 meV/unit cell, and the spin spiral chirality direction is the same as that of the field; see the insets to Fig. 4(d). It therefore can be concluded that the external electric field can tune the spin spiral induced electric polarization, and simultaneously reverse the spin spiral chirality of the *Y*-AFM ground state. We refer to this phenomenon as the polarization-chirality locking effect. In this sense, for $MnRe_2O_8$ ML the noncollinear magnetic state is electrically switchable, which is highly appealing for practical applications. In closing, we conclude that type-II multiferroic $MnRe_2O_8$ ML implies fast response, low energy consumption, and flexible magnetoelectric switching, significantly broadening its applications in such as spintronics and quantum memory.

It should be pointed out that $MnRe_2O_8$ BL with *Y*-AFM state also exhibits spin spiral order induced electric polarization. In Fig. S5(a) [48], the structure of $MnRe_2O_8$ BL following the stacking pattern as in its bulk phase is shown. In order to determine the magnetic ground state, interlayer collinear FM and AFM states, noncollinear *Y*-AFM states with the spin spiral chirality of each layer pointing upwards (UU), downwards (DD), and in opposite direction (DU) are taken into account. In accordance to our calculation results, we find that the total energy of the UU state is 0, 0.11, 13.27, and 13.14 meV/unit cell lower than those of the DD, DU, FM, and AFM states, respectively. It indicates that the energetically degenerate UU and DD states are the magnetic ground state of $MnRe_2O_8$ BL. In this case, the out-of-plane electric polarization is $-0.05/0.05$ pC/m for the UU/DD state.

In Fig. S5(b) [48], it can be observed that the induced electric polarization displays a linear dependence on λ_{SOC}, as in the ML case. It reveals that the origin of the electric polarization in the BL structure is also the noncollinear spin configuration. In addition, the polarization-chirality locking effect also exists in $MnRe_2O_8$ BL. It can be found from Fig. S5(c) [48] that the energetic degeneracy of the UU and DD states can be lifted by an external electric field. In the case of applying a field of 0.5 V/Å, for instance, the energy difference between two states reaches 2.45 meV/unit cell, and the direction of the spin spiral chirality in both monolayers can be tuned to the same direction as the external electric field. It therefore can be concluded that electrical control of noncollinear magnetism can also be achieved in $MnRe_2O_8$ BL.

IV. CONCLUSIONS

In summary, $MnRe_2O_8$ ML has been identified as a type-II multiferroic material with strong magnetoelectric coupling, especially with an out-of-plane electric polarization of $31.46\,\mu\text{C/m}^2$. It has been found that compressive strain can strengthen the supersuperexchange interaction, leading to a significantly increased Néel temperature (63 K under strain of -8%). In addition, compressive strain can also increase the polarization (e.g., $47.24\,\mu\text{C/m}^2$ as the strain is -8%). It is of high interest and great importance that a vertical electric field can modulate the spin spiral order induced electric polarization and reverse the spin spiral chirality. In other words, there is a polarization-chirality locking effect, realizing the flexibly switchable magnetism through an electric field. It therefore can be concluded that our results provide a platform for investigating the magnetoelectric physics in 2D type-II multiferroic materials and open a door for the development of magnetoelectric and magneto-optical devices in nanoscale.

ACKNOWLEDGMENTS

This work was supported by the National Natural Science Foundation of China (Grants No. 52272223 and No. 12074217), and the Shandong Provincial Key Research and Development Program (the Major Scientific and Technological Innovation Project) (Project No. 2019JZZY010302).

[1] Z. Fei, W. Zhao, T. A. Palomaki, B. Sun, M. K. Miller, Z. Zhao, J. Yan, X. Xu, and D. H. Cobden, Ferroelectric switching of a two-dimensional metal, Nature (London) **560**, 336 (2018).

[2] Y. Wei, L. Li, W. Fang, R. Long, and O. V. Prezhdo, Weak donor–acceptor interaction and interface polarization define photoexcitation dynamics in the MoS_2/TiO_2 composite: Time-domain *ab initio* simulation, Nano Lett. **17**, 4038 (2017).

[3] X. Cai, W. Yi, J. Chen, L. Lu, B. Sun, Y. Ni, S. A. T. Redfern, H. Wang, Z. Chen, and Y. Chen, A novel 2D porous C_3N_2 framework as a promising anode material with ultra-high specific capacity for lithium-ion batteries, J. Mater. Chem. A **10**, 6551 (2022).

[4] X. Zhu, X. Zhou, Y. Jing, and Y. Li, Electrochemical synthesis of urea on MBenes, Nat. Commun. **12**, 4080 (2021).

[5] Y. Wang, X. Xu, X. Zhao, W. Ji, Q. Cao, S. Li, and Y. Li, Switchable half-metallicity in A-type antiferromagnetic NiI_2 bilayer coupled with ferroelectric In_2Se_3, Npj Comput. Mater. **8**, 218 (2022).

[6] X. Xu, T. Zhong, N. Zuo, Z. Li, D. Li, L. Pi, P. Chen, M. Wu, T. Zhai, and X. Zhou, High-T_C two-dimensional ferroelectric $CuCrS_2$ grown via chemical vapor deposition, ACS Nano **16**, 8141 (2022).

[7] T. Zhang, Y. Ma, L. Yu, B. Huang, and Y. Dai, Direction-control of anisotropic electronic behaviors via ferroelasticity in two-dimensional α -MPI (M = Zr, Hf), Mater. Horiz. **6**, 1930 (2019).

[8] C. Xu, J. Mao, X. Guo, S. Yan, Y. Chen, T. W. Lo, C. Chen, D. Lei, X. Luo, J. Hao, C. Zheng, and Y. Zhu, Two-dimensional ferroelasticity in van der Waals β' -In_2Se_3, Nat. Commun. **12**, 3665 (2021).

[9] T. Lan, B. Ding, Z. Huang, F. Bian, Y. Pan, H. M. Cheng, and B. Liu, Collective behavior induced highly sensitive magneto-optic effect in 2D inorganic liquid crystals, J. Am. Chem. Soc. **143**, 12886 (2021).

[10] J. Shang, X. Tang, Y. Gu, A. V. Krasheninnikov, S. Picozzi, C. Chen, and L. Kou, Robust magnetoelectric effect in the decorated graphene/In_2Se_3 heterostructure, ACS Appl. Mater. Interfaces **13**, 3033 (2021).

[11] H. Yang, S. O. Valenzuela, M. Chshiev, S. Couet, B. Dieny, B. Dlubak, A. Fert, K. Garello, M. Jamet, D.-E. Jeong, K. Lee, T. Lee, M.-B. Martin, G. S. Kar, P. Sénéor, H.-J. Shin, and S. Roche, Two-dimensional materials prospects for non-volatile spintronic memories, Nature (London) **606**, 663 (2022).

[12] H. Tan, M. Li, H. Liu, Z. Liu, Y. Li, and W. Duan, Two-dimensional ferromagnetic-ferroelectric multiferroics in violation of the d^0 rule, Phys. Rev. B **99**, 195434 (2019).

[13] H. Ai, F. Li, H. Bai, D. Liu, K. Ho Lo, S. Yang, Y. Kawazoe, and H. Pan, Ferroelectricity coexisted with *p*-orbital ferromagnetism and metallicity in two-dimensional metal oxynitrides, Npj Comput. Mater. **8**, 60 (2022).

[14] K. Chen, J. Deng, Y. Yan, Q. Shi, T. Chang, X. Ding, J. Sun, S. Yang, and J. Z. Liu, Diverse electronic and magnetic properties of CrS_2 enabling strain-controlled 2D lateral heterostructure spintronic devices, Npj Comput. Mater. **7**, 79 (2021).

[15] S. Yu, Y. Wang, S. Wang, H. Zhang, B. Huang, Y. Dai, and W. Wei, Robust intrinsic multiferroicity in a $FeHfSe_3$ layer, J. Phys. Chem. Lett. **12**, 8882 (2021).

[16] Y. Lai, Z. Song, Y. Wan, M. Xue, C. Wang, Y. Ye, L. Dai, Z. Zhang, W. Yang, H. Du, and J. Yang, Two-dimensional ferromagnetism and driven ferroelectricity in van der Waals $CuCrP_2S_6$, Nanoscale **11**, 5163 (2019).

[17] R. Du, Y. Wang, M. Cheng, P. Wang, H. Li, W. Feng, L. Song, J. Shi, and Jun He, Two-dimensional multiferroic material of metallic p-doped SnSe, Nat. Commun. **13**, 6130 (2022).

[18] H. Yang, L. Pan, M. Xiao, J. Fang, Y. Cui, and Z. Wei, Iron-doping induced multiferroic in two-dimensional In_2Se_3, Sci. China Mater. **63**, 421 (2020).

[19] S. Liang, T. Xie, N. A. Blumenschein, T. Zhou, T. Ersevim, Z. Song, J. Liang, M. A. Susner, B. S. Conner, S.-J. Gong, J.-P. Wang, M. Ouyang, I. Žutić, A. L. Friedman, X. Zhang, and C. Gong, Small-voltage multiferroic control of two-dimensional magnetic insulators, Nat. Electron. **6**, 199 (2023).

[20] K. Adachi, K. Takeda, F. Matsubara, M. Mekata, and T. Haseda, Magnetic ordering in a partially frustrated triangular antiferromagnet $RbFeBr_3$, J. Phys. Soc. Jpn. **52**, 2202 (1983).

[21] K. F. Wang, J. M. Liu, and Z. F. Ren, Multiferroicity: The coupling between magnetic and polarization orders, Adv. Phys. **58**, 321 (2009).

[22] D. E. Cox, Neutron-diffraction determination of magnetic structures, IEEE Trans. Magn. **8**, 161 (1972).

[23] M. Lee, E. S. Choi, X. Huang, J. Ma, C. R. Dela Cruz, M. Matsuda, W. Tian, Z. L. Dun, S. Dong, and H. D. Zhou, Magnetic phase diagram and multiferroicity of $Ba_3MnNb_2O_9$: A spin-5/2 triangular lattice antiferromagnet with weak easy-axis anisotropy, Phys. Rev. B **90**, 224402 (2014).

[24] D.-L. Bao, A. O'Hara, S. X. Du, and S. T. Pantelides, Tunable, ferroelectricity-inducing, spin-spiral magnetic ordering in monolayer FeOCl, Nano Lett. **22**, 3598 (2022).

[25] S. Ishiwata, Y. Taguchi, H. Murakawa, Y. Onose, and Y. Tokura, Low-magnetic-field control of electric polarization vector in a helimagnet, Science **319**, 1643 (2008).

[26] S. Nakatsuji, N. Kiyohara, and T. Higo, Large anomalous Hall effect in a non-collinear antiferromagnet at room temperature, Nature (London) **534**, S5 (2016).

[27] H. Ju, Y. Lee, K. T. Kim, I. H. Choi, C. J. Roh, S. Son, P. Park, J. H. Kim, T. S. Jung, J. H. Kim, K. H. Kim, J. G. Park, and J. S. Lee, Possible persistence of multiferroic order down to bilayer limit of van der Waals material NiI_2, Nano Lett. **21**, 5126 (2021).

[28] P. Qin, Z. Feng, X. Zhou, H. Guo, J. Wang, H. Yan, X. Wang, H. Chen, X. Zhang, H. Wu, Z. Zhu, and Z. Liu, Anomalous Hall effect, robust negative magnetoresistance, and memory devices based on a noncollinear antiferromagnetic metal, ACS Nano **14**, 624 (2020).

[29] N. Terada, D. D. Khalyavin, J. M. Perez-Mato, P. Manuel, D. Prabhakaran, A. Daoud-Aladine, P. G. Radaelli, H. S. Suzuki, and H. Kitazawa, Magnetic and ferroelectric orderings in multiferroic α-$NaFeO_2$, Phys. Rev. B **89**, 184421 (2014).

[30] S. Hu, D.-F. Shao, H. Yang, M. Tang, Y. Yang, W. Fan, S. Zhou, E. Y. Tsymbal, and X. Qiu, Efficient perpendicular magnetization switching by a magnetic spin Hall effect in a noncollinear antiferromagnet, Nat. Commun. **13**, 4447 (2022).

[31] Z. Q. Liu, H. Chen, J. M. Wang, J. H. Liu, K. Wang, Z. X. Feng, H. Yan, X. R. Wang, C. B. Jiang, J. M. D. Coey, and A. H. MacDonald, Electrical switching of the topological anomalous Hall effect in a non-collinear antiferromagnet above room temperature, Nat. Electron. **1**, 172 (2018).

[32] T. Finger, D. Senff, K. Schmalzl, W. Schmidt, L. P. Regnault, P. Becker, L. Bohatý, and M. Braden, Electric-field control of the

chiral magnetism of multiferroic $MnWO_4$ as seen via polarized neutron diffraction, Phys. Rev. B **81**, 054430 (2010).

[33] J. J. Zhang, L. Lin, Y. Zhang, M. Wu, B. I. Yakobson, and S. Dong, Type-II multiferroic $Hf_2VC_2F_2$ MXene monolayer with high transition temperature, J. Am. Chem. Soc. **140**, 9768 (2018).

[34] A. O. Fumega and J. L. Lado, Microscopic origin of multiferroic order in monolayer NiI_2, 2D Mater. **9**, 025010 (2022).

[35] G. G. Kresse and J. J. Furthmüller, Efficient iterative schemes for *ab initio* total-energy calculations using a plane-wave basis set, Phys. Rev. B **54**, 11169 (1996).

[36] G. Kresse and D. Joubert, From ultrasoft pseudopotentials to the projector augmented-wave method, Phys. Rev. B **59**, 1758 (1999).

[37] J. P. Perdew, K. Burke, and M. Ernzerhof, Generalized gradient approximation made simple, Phys. Rev. Lett. **77**, 3865 (1996).

[38] B. C. Gong, H. C. Yang, J. F. Zhang, K. Liu, and Z. Y. Lu, Inducing high-T_c ferromagnetism in the van der Waals crystal $Mn(ReO_4)_2$ via charge doping: A first-principles study, Phys. Rev. B **104**, 075133 (2021).

[39] S. Mehmood and Z. Ali, DFT study of the spin glass and ferrimagnetism in quadruple perovskites $CaCu_3B_2Ir_2O_{12}$ (B = Mn, Fe, Co, and Ni) for spintronic applications, Appl. Phys. A **129**, 76 (2023).

[40] H. J. Monkhorst and J. D. Pack, Special points for Brillouin-zone integrations, Phys. Rev. B **13**, 5188 (1976).

[41] A. Togo and I. Tanaka, First principles phonon calculations in materials science, Scr. Mater. **108**, 1 (2015).

[42] C. Huang, J. Feng, J. Zhou, H. Xiang, K. Deng, and E. Kan, Ultra-high-temperature ferromagnetism in intrinsic tetrahedral semiconductors, J. Am. Chem. Soc. **141**, 12413 (2019).

[43] S. Chib and E. Greenberg, Understanding the metropolis-hastings algorithm, Am. Stat. **49**, 327 (1995).

[44] M. Newman and G. T. Barkema, *Monte Carlo Methods in Statistical Physics* (Oxford University Press, Oxford, 1999).

[45] L. Liu, X. Ren, J. Xie, B. Cheng, W. Liu, T. An, H. Qin, and J. Hu, Magnetic switches via electric field in BN nanoribbons, Appl. Surf. Sci. **480**, 300 (2019).

[46] A. Butz, G. Miehe, H. Paulus, P. Strauss, and H. Fuess, The crystal structures of $Mn(ReO_4)_2 \cdot 2H_2O$ and of the anhydrous perrhenates $M(ReO_4)_2$ of divalent manganese, cobalt, nickel, and zinc, J. Solid State Chem. **138**, 232 (1998).

[47] C. C. Torardi, W. M. Reiff, B. C. Dodrill, and T. Vogt, Layered 3-D ferromagnets and antiferromagnets, $M^{2+}(ReO_4)_2$ (M = Mn, Fe, Co, Ni, Cu): Importance of dipolar interactions, Mat. Res. Soc. Symp. Proc. **453**, 399 (1997).

[48] See Supplemental Material at http://link.aps.org/supplemental/10.1103/PhysRevB.108.174429 for (i) total energy of $MnRe_2O_8$ ML with different magnetic states; (ii) AIMD results; (iii) phonon dispersion of $MnRe_2O_8$ ML with different magnetic states; (iv) band structure, partial charge density, and PDOS of $MnRe_2O_8$ ML; (v) crystal structure, the relationship between electric polarization and strength of SOC, and the effect of external electric field on the energy difference ΔE_{UU-DD} of $MnRe_2O_8$ BL.

[49] S. Seki, Y. Onose, and Y. Tokura, Spin-driven ferroelectricity in triangular lattice antiferromagnets $ACrO_2$(A = Cu, Ag, Li, or Na), Phys. Rev. Lett. **101**, 067204 (2008).

[50] M. Kenzelmann, G. Lawes, A. B. Harris, G. Gasparovic, C. Broholm, A. P. Ramirez, G. A. Jorge, M. Jaime, S. Park, Q. Huang, A. Ya. Shapiro, and L. A. Demianets, Direct transition from a disordered to a multiferroic phase on a triangular lattice, Phys. Rev. Lett. **98**, 267205 (2007).

[51] J. Hwang, E. S. Choi, F. Ye, C. R. Dela Cruz, Y. Xin, H. D. Zhou, and P. Schlottmann, Successive magnetic phase transitions and multiferroicity in the spin-one triangular-lattice antiferromagnet $Ba_3NiNb_2O_9$, Phys. Rev. Lett. **109**, 257205 (2012).

[52] J. Kanamori, Superexchange interaction and symmetry properties of electron orbitals, J. Phys. Chem. Solids. **10**, 87 (1959).

[53] R. Rawl, M. Lee, E. S. Choi, G. Li, K. W. Chen, R. Baumbach, C. R. dela Cruz, J. Ma and H. D. Zhou, Magnetic properties of the triangular lattice magnets $A_4B'B_2O_{12}$ (A = Ba, Sr, La; B′ = Co, Ni, Mn; B = W, Re), Phys. Rev. B **95**, 174438 (2017).

[54] Z. Lu, L. Ge, G. Wang, M. Russina, G. Günther, C. R. dela Cruz, R. Sinclair, H. D. Zhou, and J. Ma, Lattice distortion effects on the frustrated spin-1 triangular-antiferromagnet $A_3NiNb_2O_9$ (A = Ba, Sr, and Ca), Phys. Rev. B **98**, 094412 (2018).

[55] J. Jiao, S. Zhang, O. Huang, M. Zhang, M. Shu, G. Lin, C. dela Cruz, V. Garlea, N. Butch, M. Matsuda, H. Zhou and J. Ma, Quantum effect on the ground state of the triple-perovskite $Ba_3MNb_2O_9$ (M = Co, Ni, and Mn) with triangular-lattice, Chem. Mater. **34**, 6617 (2022).

[56] M.-H. Whangbo, H.-J. Koo, and D. Dai, Interpretation of the magnetic structures of $Cu_2Te_2O_5X_2$ (X = Cl, Br) and $Ca_{3.1}Cu_{0.9}RuO_6$ on the basis of electronic structure considerations: Cases for strong super-superexchange interactions involving Cu^{2+} ions, Inorg. Chem. **42**, 3898 (2003).

[57] H.-J. Koo, M.-H. Whangbo, P. D. VerNooy, C. C. Torardi, and W. J. Marshall, Flux growth of vanadyl pyrophosphate, $(VO)_2P_2O_7$, and spin dimer analysis of the spin exchange interactions of $(VO)_2P_2O_7$ and vanadyl hydrogen phosphate, $VO(HPO_4) \cdot 0.5\,H_2O$, Inorg. Chem. **41**, 4664 (2002).

[58] W. A. Harrison, *Electronic Structure and the Properties of Solids* (Dover, New York, 1989).

[59] J.-S. Zhou and J. B. Goodenough, Intrinsic structural distortion in orthorhombic perovskite oxides, Phys. Rev. B **77**, 132104 (2008).

[60] C. Wang, H. Seinige, G. Cao, J.-S. Zhou, J. B. Goodenough, and M. Tsoi, Electrically tunable transport in the antiferromagnetic Mott insulator Sr_2IrO_4, Phys. Rev. B **92**, 115136 (2015).

[61] J. Ma, C. D. Dela Cruz, T. Hong, W. Tian, A. A. Aczel, S. X. Chi, J. Q. Yan, Z. L. Dun, H. D. Zhou, and M. Matsuda, Magnetic phase transition in the low-dimensional compound $BaMn_2Si_2O_7$, Phys. Rev. B **88**, 144405 (2013).

[62] J.-S. Zhou, J. A. Alonso, V. Pomjakushin, J. B. Goodenough, Y. Ren, J.-Q. Yan, and J.-G. Cheng, Intrinsic structural distortion and superexchange interaction in the orthorhombic rare-earth perovskites $RCrO_3$, Phys. Rev. B **81**, 214115 (2010).

[63] D. Di Sante, A. Stroppa, P. Barone, M.-H. Whangbo, and S. Picozzi, Emergence of ferroelectricity and spin-valley properties in two-dimensional honeycomb binary compounds, Phys. Rev. B **91**, 161401(R) (2015).

[64] C. Huang, J. Zhou, H. Sun, F. Wu, Y. Hou, and E. Kan, Toward room-temperature electrical control of magnetic order in multiferroic van der Waals materials, Nano Lett. **22**, 5191 (2022).

[65] Y. Wan, T. Hu, X. Mao, J. Fu, K. Yuan, Y. Song, X. Gan, X. Xu, M. Xue, X. Cheng, C. Huang, J. Yang, L. Dai, H. Zeng, and E. Kan, Room-temperature ferroelectricity in 1T′-ReS_2 multilayers, Phys. Rev. Lett. **128**, 067601 (2022).

[66] S. Dong, J.-M. Liu, S.-W. Cheong, and Z. Ren, Multiferroic materials and magnetoelectric physics: Symmetry, entanglement, excitation, and topology, Adv. Phys. **64**, 519 (2015).

[67] H. J. Xiang, E. J. Kan, Y. Zhang, M.-H. Whangbo, and X. G. Gong, General theory for the ferroelectric polarization induced by spin-spiral order, Phys. Rev. Lett. **107**, 157202 (2011).

[68] J. T. Zhang, C. Ji, J. L. Wang, W. S. Xia, B. X. Guo, X. M. Lu, and J. S. Zhu, Spin-induced ferroelectricity in a triangular-lattice antiferromagnet studied by magnetoelectric coupling tensors, Phys. Rev. B **96**, 235136 (2017).